Impurity Transport Studies at Wendelstein 7-X by Means of X-ray Imaging Spectrometer Measurements[a)]

A. Langenberg,[1, b)] F. Warmer,[1] G. Fuchert,[1] O. Marchuk,[2] A. Dinklage,[1] Th. Wegner,[1] J.A. Alonso,[3] S. Bozhenkov,[1] K.J. Brunner,[1] R. Burhenn,[1] B. Buttenschön,[1] P. Drews,[2] B. Geiger,[1] O. Grulke,[1, 4] M. Hirsch,[1] U. Höfel,[1] K.P. Hollfeld,[2] C. Killer,[1] J. Knauer,[1] T. Krings,[2] F. Kunkel,[1] U. Neuner,[1] G. Offermanns,[2] N.A. Pablant,[5] E. Pasch,[1] K. Rahbarnia,[1] G. Satheeswaran,[2] J. Schilling,[1] B. Schweer,[2] H. Thomsen,[1] P. Traverso,[6] R.C. Wolf,[1] and the W7-X Team[c)]

[1)] *Max-Planck-Institut für Plasmaphysik, 17491 Greifswald, Germany*

[2)] *Forschungszentrum Jülich GmbH, Institut für Energie- und Klimaforschung - Plasmaphysik, 52425 Jülich, Germany*

[3)] *Laboratorio Nacional de Fusión, Asociación EURATOM-CIEMAT, Madrid, Spain*

[4)] *Technical University of Denmark DTU, Dept Phys, PPFE, DK-2800 Lyngby, Denmark*

[5)] *Princeton Plasma Physics Laboratory, Princeton, NJ, USA*

[6)] *Auburn University, Auburn, Alabama, USA*

(Dated: 6 November 2018)

This paper reports on the effect of on- and off-axis heating power deposition on the impurity confinement in purely electron cyclotron resonance heated He plasmas on the stellarator Wendelstein 7-X. Therefore, impurity transport times τ_I have been determined after Fe impurity injections by laser ablations and monitoring the temporal impurity emissivities by the x-ray imaging spectrometer HR-XIS. A significant increase of τ_I has been observed when changing the power deposition from on- to off-axis heating with energy confinement times τ_E being mainly unaffected. In addition, the scaling of impurity transport properties with respect to a variation of heating power P_{ECRH} and electron density n_e has been investigated by keeping the heating power deposition on-axis. The observed τ_I scaling compares well to known τ_I scaling laws observed in other machines. A comparison of τ_I and τ_E yields an averaged ratio of $\tau_E/\tau_I = 1.3$ and transport times in the range of τ_I=40-130 ms and τ_E=40-190 ms. Comparing those absolute values to neoclassical predictions supports the recently observed nature of anomalous transport in Wendelstein 7-X, given within the up to now investigated operational parameters.

PACS numbers: Valid PACS appear here

I. INTRODUCTION

Due to non axis-symmetric 3D magnetic fields, impurity transport in the hot plasma core in stellarators is expected to differ from that in tokamaks. In view of reactor-like operation, understanding the impurity transport is a prerequisite for steady-state operation, especially for stellarators. These aspects motivate initial impurity transport studies in Wendelstein 7-X (W7-X) at previously - in optimized stellarators – unexplored, reactor-relevant collisionalities. New effects, like potential variations on flux-surfaces[1] or screening effects due to species dependent transport regimes[2] are examples for aspects which attracted recent interest. The ability of W7-X for long pulse operation under fusion relevant plasma conditions offers unique possibilities to study impurity transport even on large transport time scales.

Experimentally, impurity transport investigations have been performed using several techniques, as *e.g.* monitoring the spatial and/or temporal emissivities of pulsed impurity injections[3–7] or intrinsic impurities[8,9]. From the experimental data, several transport relevant plasma parameters as the impurity transport time τ_I[10,11], the diffusive and convective transport parameters D and v[12–18] or the radial electric field E_r[19], can be determined either directly or from a comparison with transport code calculations.

For an initial, fundamental characterization of transport processes of the recently commissioned W7-X machine[20], this paper presents results of the impurity and energy confinement behavior along the ultimate goal of maximized energy and minimized impurity confinement. As in many large scale fusion experiments, an empirical scaling of the impurity confinement with heating power P_{ECRH} and electron density n_e has been observed[3,6], initial systematic P_{ECRH} - n_e scans have been performed at W7-X in Helium plasmas within two different magnetic configurations comparing measured impurity transport and energy confinement times. Furthermore, the impact of the specific settings of the heating power deposition on the impurity confinement has been investigated.

[a)] Invited paper published as part of the Proceedings of the 45th Conference on Plasma Physics (EPS), Prague, Czech Republic, July, 2018.

[b)] andreas.langenberg@ipp.mpg.de

[c)] R.C. Wolf *et al.* Nuclear Fusion **57**, 102020 (2017).

II. EXPERIMENTAL SETUP

For the investigation of impurity transport properties in W7-X, non recycling Fe impurities have been injected into the plasma using a Laser Blow-off (LBO) system[11]. After injection, the spatio-temporal evolution of impurities has been monitored using two X-ray imaging spectrometer systems, namely the X-ray Imaging Crystal Spectrometer (XICS) and the High Resolution X-ray Imaging Spectrometer (HR-XIS)[10,21]. The temporal evolution of the recorded brightness of selected impurity emission lines gives rise to impurity transport times τ_I, being a direct measure of global impurity transport properties[10].

A. Laser Blow-off System

The injection of non recycling, mainly metallic impurities such as Al, Ti, Fe, Mo, W, and Si is realized using the laser blow-off technology. Here, atoms, clusters, and macroscopic particles are ablated out of a 2-5 μm thick material layer covering a glass target by firing a laser onto the target. The laser used at W7-X is a Nd:YAG laser with 1 J laser energy and a maximum repetition rate of 20 Hz. It is guided onto the target holder via several mirrors with the last mirror being steerable allowing to adjust the laser spot position on the target. The glass target holder can mount up to 4 glass targets and is located 65 cm away from the last closed flux surface of the magnetic standard configuration[22]. An observation camera installed behind the target holder allows an observation of the evaporation process. Depending on the target material, its thickness and the laser spot diameter, impurities in the order of $1{\times}10^{18}$ particles can be evaporated per laser pulse. The detailed design and performance of the system has been described by Wegner *et al.*[11].

B. Imaging Spectrometers XICS and HR-XIS

The imaging spectrometers XICS and HR-XIS are equipped with several different crystals for the observation of the X-ray emission of various impurity species in highly ionized charge states. Making use of the imaging properties of a spherical bent crystal, X-rays emitted from the plasma impurities are imaged onto a two dimensional detector area, yielding energy and spatial resolution in horizontal and vertical direction on the detector. A spectral fit[23] and a tomographic inversion[12,24] of recorded spectra provides radial profiles of the impurity density $n_Z(\rho)$, ion and electron temperature, $T_i(\rho)$ and $T_e(\rho)$, and plasma rotation $v(\rho)$ with ρ defined as the square root of the magnetic flux ψ, normalized to the last closed flux surface: $\rho = \sqrt{(\psi/\psi_{LCFS})}$. For this study, the emission of He-like Fe (FeXXV) has been monitored with a Ge(422) crystal under a Bragg angle of 53.61° using the HR-XIS system. With a viewing geometry from the plasma center towards well above the mid plasma radius ($\rho = 0 - 0.6$) and a maximal time resolution of $t = 2$ ms, HR-XIS is well suited for transport investigations of impurities located in the bulk plasma. A detailed description of the design and the performance of both spectrometers can be found in Ref.[10].

III. GLOBAL IMPURITY TRANSPORT AT W7-X

This section discusses global transport properties of W7-X based on measurements of impurity transport times τ_I and energy confinement times τ_E within a systematic scan of the electron density n_e and the electron cyclotron resonance (ECR) heating power P_{ECRH}. It should be mentioned that the purity of the investigated He plasmas is to some extend reduced, with usual H gas concentrations between 5-30 % as evident from measurements of the edge He and H densities, possibly affecting the here discussed absolute values of τ_I and τ_E.

A. Measurement of Impurity Transport Times

As reported in previous works[10,11], the measurement of the exponential decay of the impurity signal after a pulsed impurity injection allows to determine the impurity transport time τ_I that is closely related to impurity transport properties. According to Ref.[10], τ_I is defined as the time constant of the exponential decaying impurity signal after achieving an ionization equilibrium[10,11]. Since the impurity signal varies with T_e and n_e, we timed the laser pulses for impurity injection within the flat top phase of the experiment with stationary conditions for both T_e and n_e.
Fig.1 shows typical time traces of a centrally ECR heated experimental program with a single Fe injection, showing the total heating power P_{ECRH}, the line of sight integrated electron density n_e measured by the interferometer, the central T_e and T_i values as measured by the electron cyclotron emission and XICS diagnostics, and the Fe^{24+} line brightness observed with the HR-XIS spectrometer. The distinct peak in the Fe^{24+} signal at $t = 1.6$ s originates from a single Fe injection via the LBO system, showing the above mentioned exponential decay of the Fe^{24+} signal. The background signal level before and after the Fe injection is induced by the Bremsstrahlung background radiation. The shown time traces demonstrate stationary plasma conditions for $t \geq 1.5$ s and also the non perturbing character of the injected Fe tracer impurity.

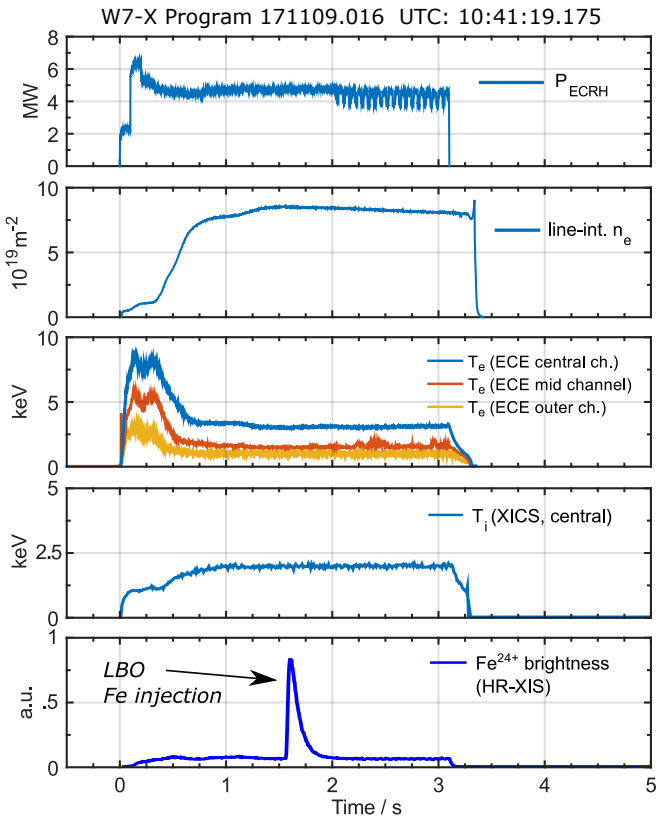

FIG. 1. Time traces of a centrally ECR heated experimental program in the magnetic standard configuration of W7-X showing the total ECR heating power P_{ECRH}, line of sight integrated density n_e, central, mid, and outer radius electron temperatures, central ion temperature, and the brightness of He-like iron emission lines.

B. Impurity Transport Time Scaling

The empirical scaling of τ_I with respect to P_{ECRH} and n_e has been investigated in the magnetic standard configuration and the magnetic high mirror configuration of W7-X[22] by performing several experimental programs similar to that shown in Fig.1. The label 'high mirror' refers to the higher magnetic mirror term of that configuration compared to the W7-X standard configuration, see also[25]. For the transport analysis, P_{ECRH} and n_e have been scanned systematically from the lowest possible values up to the maximum available heating power and the appearance of a density limit, terminating the experimental program by a radiation collapse[26]. All programs have been performed with the working gas helium. The obtained τ_I values are shown in color code in Fig.2 for each experimental program with the corresponding P_{ECRH} and n_e parameters. In both magnetic configurations, two clear trends can be observed. On the one hand, τ_I decreases with increasing P_{ECRH}, being well known in literature as power degradation[27–29]. Here, the increased heating power leads to a reduced confinement of impurity species. On the other hand, τ_I increases with increasing n_e. This enhanced confinement of impurities towards higher n_e has also been observed in many other machines.

For a quantitative assessment of these effects, the scaling of τ_I with P_{ECRH} and n_e has been fitted to a two dimensional function according to the typical scaling[30]

$$\tau_I \propto \gamma \cdot P_{\mathrm{ECRH}}^{\alpha} \cdot n_e^{\beta} \tag{1}$$

with the free parameters α, β, and γ. For visualization, the 2D surfaces resulting from the data fit are shown together with the discrete τ_I values in the top of Fig.3 for the standard and high mirror configurations on identical scales, respectively. As already evident from the figure, the scaling of τ_I with P_{ECRH} and n_e is very similar for both magnetic configurations. In fact, the determined values for the fit parameters γ, α, and β are identical for the standard and the high mirror configuration within the experimental uncertainties as listed in Tab.I. The bottom of Fig.3 compares measured τ_I values to predicted ones τ_I^{REG} according to the scaling law (Eq.1), yielding coefficients of determination (CoD) of 0.66 and 0.75 for the standard and high mirror configurations, respectively.

C. Energy Confinement Time Scaling

In analogy to the impurity transport time, also the energy confinement time τ_E is expected to scale according to Eq.1[6]. For the validation of a desired maximized energy and at the same time minimized impurity confinement, τ_E has been determined for the experimental programs of the $P_{\mathrm{ECRH}} - n_e$ scans discussed in section III B for both magnetic configurations standard and high mirror. The τ_E values have been evaluated using the diamagnetic plasma energy W_{dia} as measured by the diamagnetic loop diagnostic[31] and the total heating power P_{ECRH}:

$$\tau_E = W_{\mathrm{dia}} / \left(P_{\mathrm{ECRH}} - dW_{\mathrm{dia}}/dt\right). \tag{2}$$

To improve statistics, here τ_E has been evaluated at several time points within the experimental programs, providing more data points for the P_{ECRH} - n_e scan compared to the impurity transport times evaluated only at times of impurities injected with the LBO.

The resulting τ_E values show a pronounced scaling with P_{ECRH} and n_e, very similar to that obtained for τ_I, including the effects of power degradation with increasing P_{ECRH} and improved confinement with increasing n_e[32]. A quantitative analysis (compare section III B) yields the scaling parameters listed in Tab.II. The α, β, and γ values given here compare well to values derived from a more general τ_E scaling study, including all experimental programs from the last W7-X experimental campaign[32]. Fig.4 compares calculated energy confinement times τ_E^{REG} using scaling parameters given in Tab.II to actual measured ones, τ_E, with the solid line corresponding to τ_E^{REG}=τ_E. For both magnetic configurations, standard and high mirror, the scaling of τ_E is

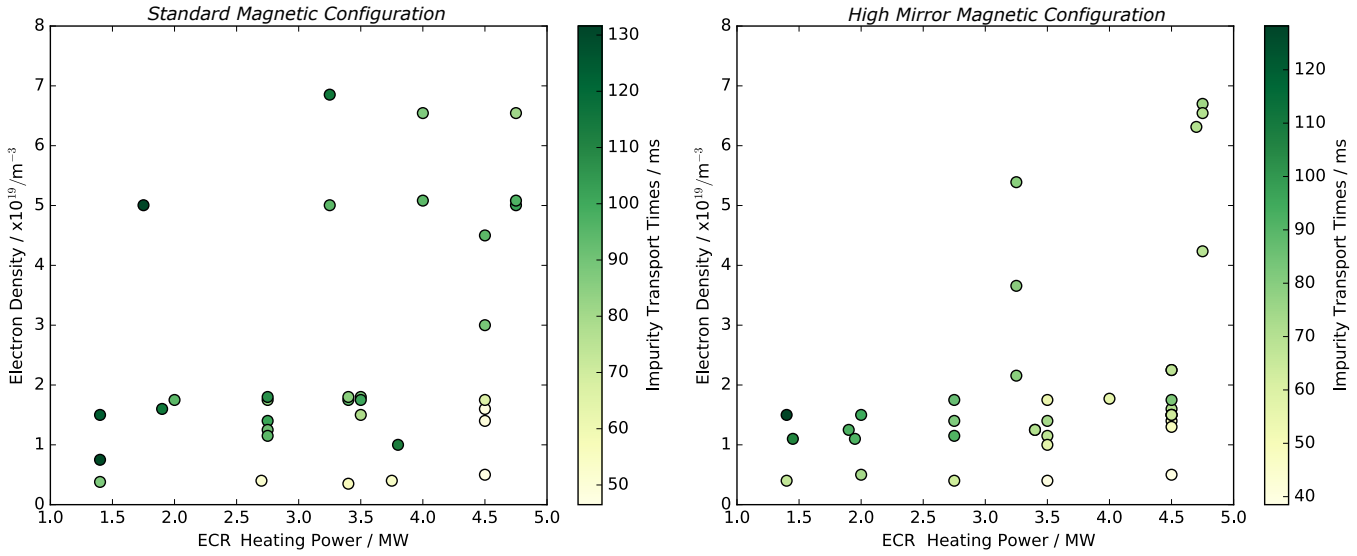

FIG. 2. Scaling of τ_I with respect to P_{ECRH} and n_e in the magnetic configurations standard (left) and high mirror (right).

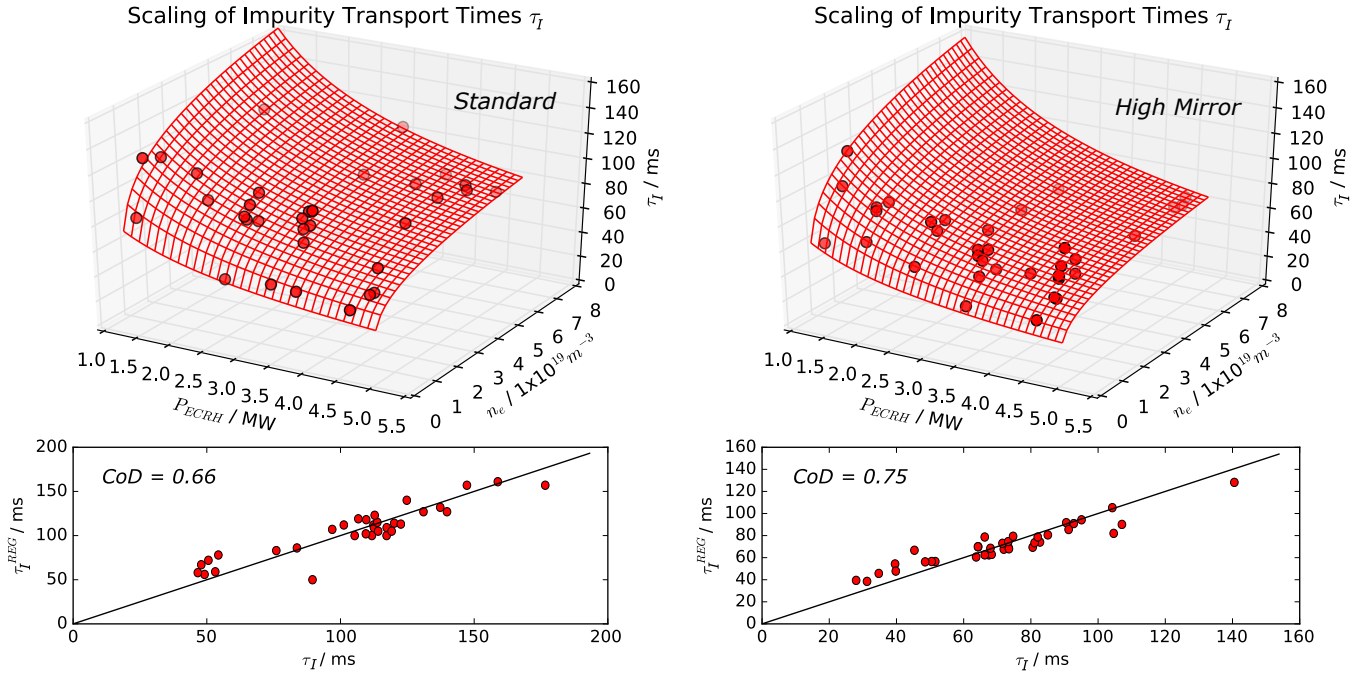

FIG. 3. Top: Fitted τ_I scaling (meshgrid) from a two dimensional least squares fit of discrete τ_I values (dots) with respect to P_{ECRH} and n_e according to Eq.1. Bottom: Linear regression curve for fitted and actual measured τ_I values in the magnetic configurations standard (left) and high mirror (right).

well described with CoD values of 0.87 and 0.91.

D. Heating Power Deposition

Additionally to the P_{ECRH} and n_e scaling of the impurity transport times, another variation of τ_I has been observed when varying the ECR heating power deposition from pure on-axis to pure off-axis heating. The different heating deposition profiles have been achieved making use of the ECRH steering launcher, installed at the W7-X ECRH system[33] that allows to deposit the heating power at different radial locations inside the plasma.
For the study of the heating power deposition effect on the impurity confinement, two identical experimental programs, 171012.018 and 171012.042 have been performed, guiding the heating power of 4 gyrotrons on

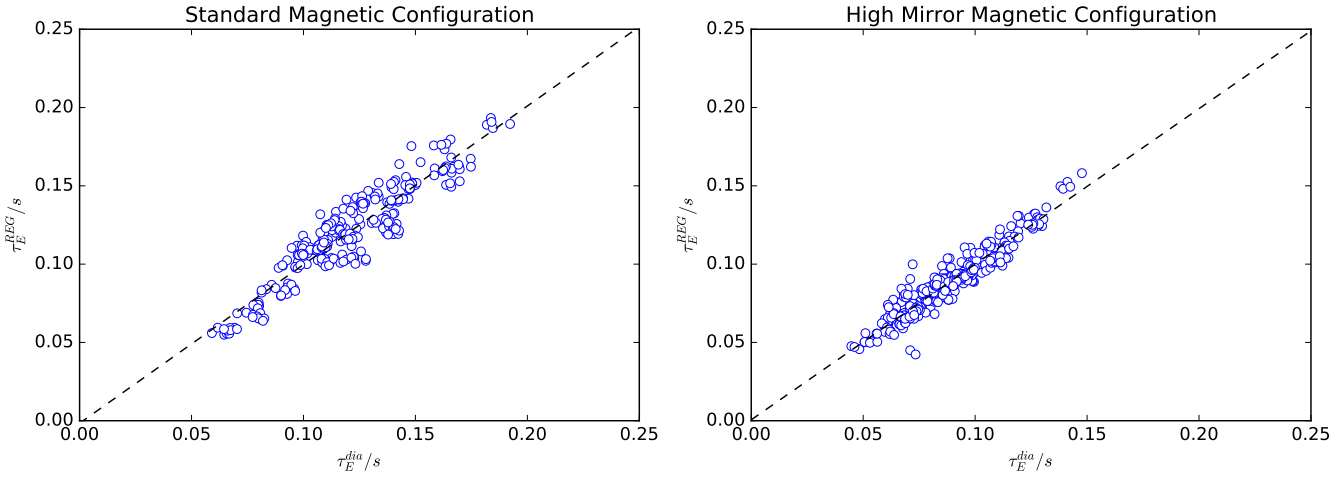

FIG. 4. Linear regression curve for fitted and actual measured τ_E values in the magnetic configurations standard (left) and high mirror (right).

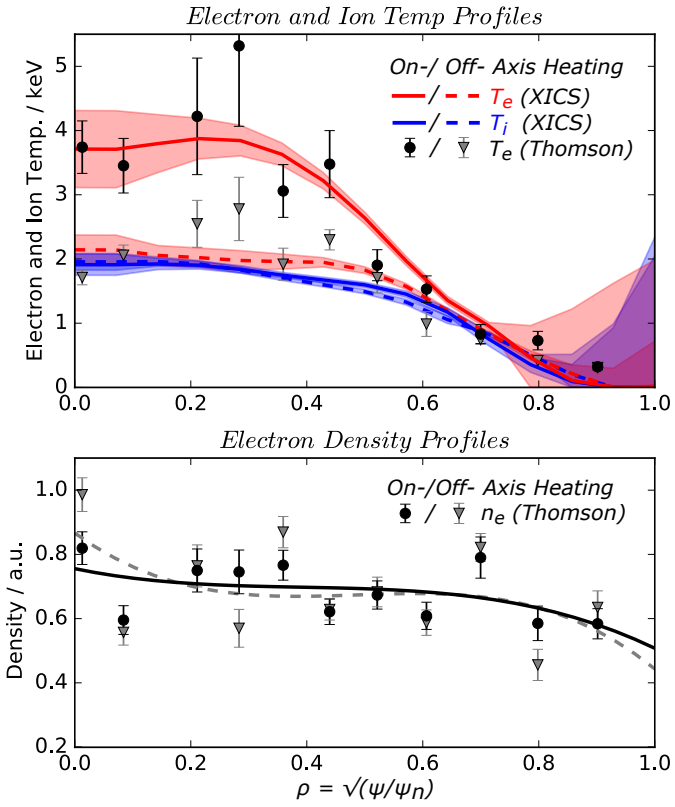

FIG. 5. Top: Ion (blue lines) and electron temperature profiles (red lines) as measured by XICS for on-axis (solid lines) and off-axis (dashed lines) ECRH power deposition together with Thomson scattering data (symbols). The shaded areas as well as the shown error bars correspond to an uncertainty of one standard deviation.
Bottom: Electron density profiles measured by the Thomson scattering system (symbols) with a spline fit of data points for on-axis (solid line) and off-axis (dashed line) power deposition.

τ_I scaling parameters	standard	high mirror
α	-0.49 ± 0.07	-0.60 ± 0.06
β	0.19 ± 0.03	0.21 ± 0.03
γ	140 ± 10	130 ± 8
CoD	0.66	0.75

TABLE I. Fitted scaling parameters α, β, and γ according to Eq.1 for the scaling of τ_I with P_{ECRH} and n_e in He plasmas for the magnetic standard and high mirror configurations. Also given is the coefficient of determination, CoD.

τ_E scaling parameters	standard	high mirror
α	-0.64 ± 0.02	-0.60 ± 0.01
β	0.23 ± 0.01	0.25 ± 0.01
γ	188 ± 2	141 ± 1
CoD	0.87	0.91

TABLE II. Fitted scaling parameters α, β, and γ according to Eq.1 for the scaling of τ_E with P_{ECRH} and n_e in He plasmas for the magnetic standard and high mirror configurations. Also given is the coefficient of determination, CoD.

radial positions pure on-axis at $\rho = 0$ and off-axis at $\rho = 0.45$ with a total heating power of $P_{\mathrm{ECRH}} = 2.0$ MW.

In both experimental programs, stationary plasma conditions as exemplarily shown in Fig.1 have been achieved with static line of sight integrated electron densities as well as static ion and electron temperatures. Fig.5 shows measured T_i, T_e, and n_e profiles for the on- and off-axis heated programs at the time of the impurity injection around $t = 1.2$ s. While the measured energy confinement times $\tau_E = 90 \pm 2$ ms, the diamagnetic plasma energy contents of $W_{\mathrm{dia}} = 185 \pm 5$ kJ as well as the T_i profiles are nearly identical for both the on- and off-axis

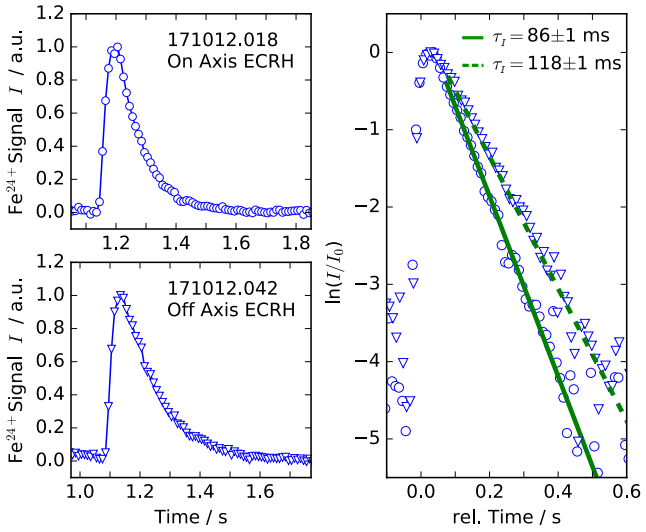

FIG. 6. Left: Time traces of Fe^{24+} line brightnesses after impurity injections for on- and off-axis ECR heating. Right: Logarithmic plot of normalized Fe^{24+} time traces and linear fits of τ_I for on-axis ECRH (solid line) and off-axis ECRH (dashed line).

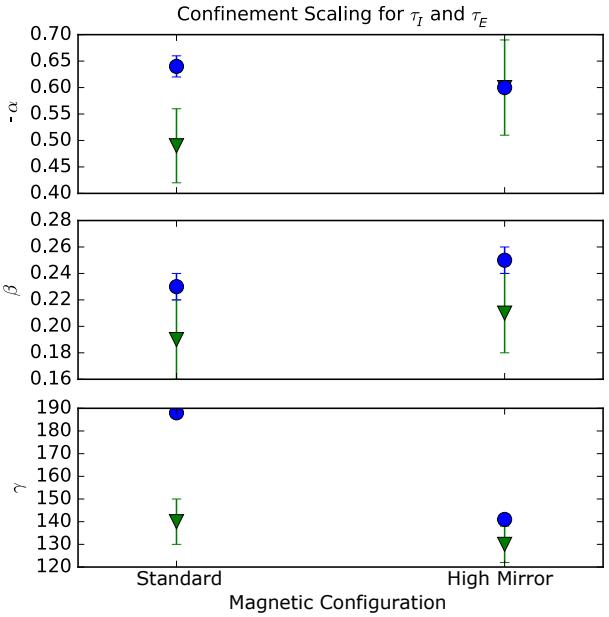

FIG. 7. Overview on the scaling parameters α, β, and γ for the τ_I (triangles) and τ_E scaling (circles) in the magnetic standard and high mirror configurations.

heated plasmas, the measured T_e profiles differ significantly from each other, as shown in the top of Fig.5. As reported from other stellarators[34] and recently also for W7-X[35], ECR off-axis heating leads to a strong flattening of the T_e profile from the plasma center up to the position of the ECRH deposition, accompanied by a peaking of the n_e profile. While also for this study, the T_e profile flattening is evident from the XICS measurements in well agreement with the Thomson scattering data[36,37], the n_e profile peaking is not significant within the scattering of profile data given in the bottom of Fig.5. However, also here an averaged increase of the n_e profile can be expected as despite the flattened, overall decreased T_e profile, the measured W_{dia} is very similar for both the on- and off-axis heated plasmas.

Regarding the impurity confinement, a significant change in τ_I can be observed when changing from on- to off-axis heating. In fact, τ_I changes from $\tau_I = 86 \pm 1$ ms for on-axis to $\tau_I = 118 \pm 1$ ms for off-axis heating, as shown in Fig.6. Here, the left of Fig.6 shows time traces of the Fe^{24+} brightness after the Fe impurity injection for on- and off-axis heating. On the right of Fig.6, a logarithmic plot of both time traces is shown together with the linear regression curves, yielding the impurity transport times given above.

A more detailed investigation, repeating the shown experimental programs with additional ECRH power deposition profiles as well as analyzing further accessible plasma parameters having impact to the impurity transport, as *e.g.* the radial electric field E_r, is ongoing and will be discussed in forthcoming publications.

IV. RESULTS AND DISCUSSION

A. Impurity and Energy Confinement

Fig.7 plots the derived scaling parameters α, β, and γ of impurity and energy confinement, see Tab.I and II, for the magnetic configurations standard and high mirror. Comparing both magnetic configurations, the global impurity confinement turns out to be nearly identical, as demonstrated by the scaling parameters α, β, and γ matching each other within the uncertainties, see Fig.7, triangles. The same is true for the scaling of the energy confinement with respect to P_{ECRH} and n_e, yielding within the uncertainties nearly equal values for α and β, see circles in Fig.7. However, the absolute τ_E values are on average slightly enhanced for the magnetic standard configuration, as evident from $\gamma_{Standard} > \gamma_{HighMirror}$, see circles in the bottom of Fig.7. In fact, the observed improved energy confinement in the magnetic standard configuration is predicted by neoclassical theory as the value of the 'effective helical ripple' ϵ_{eff}[38] is much larger in the high mirror ($\epsilon_{eff} = 2.4\%$) than in the magnetic standard configuration ($\epsilon_{eff} = 0.7\%$)[39], yielding a larger neoclassical diffusive transport parameter D_{11} in the $1/\nu$ transport regime according to $D_{11}^{1/\nu} \propto \epsilon_{eff}^{3/2}$[38] and so a reduced energy confinement for the magnetic high mirror compared to the magnetic standard configuration.

A comparison of the energy and impurity confinement shows a slightly improved energy confinement in both configurations, as reflected by the generally increased

scaling parameters: $\{\alpha,\beta,\gamma\}(\tau_E) > \{\alpha,\beta,\gamma\}(\tau_I)$. This enhanced energy confinement over impurity confinement for high Z materials has also been observed for the low confinement regimes at the Tokamaks JET and Tore Supra[6].

Results from neoclassical calculations including measured T_e, T_i, and n_e profiles[27,32] shows that neoclassical theory alone can not reproduce the experimental findings without taking into account turbulent transport. In particular, the experimentally obtained τ_E values are significantly lower than those derived from neoclassical theory, roughly in the order of 50 %[32]. A similar trend can be observed also for the impurity transport: While from neoclassical theory, the predicted diffusive transport coefficient profile $D(\rho)$ is constant along ρ with an absolute value of $D < 0.1$ m^2/s[40], the actual measured profile of $D(\rho)$ significantly rises towards the plasma edge with peaking values of $D \leq 1.5$ m^2/s as derived from recent Fe impurity transport and earlier Ar impurity transport studies at W7-X[12,40]. Both observations suggest significant turbulent contributions to the energy as well as the impurity transport within the machine parameters, W7-X has been operated so far.

B. Heating Power Deposition

In large scale fusion devices, impurities can be prevented from accumulating inside the plasma center by applying a strong central ECR heating. This pretty robust effect is well known and has been observed in several experiments[5,41]. Hence, the increased τ_I value for the off-axis ECR heating observed in this study is most probably related to a lack of the impurity pump out by centrally ECRH. As the measured T_i profiles for on- and off-axis heating are identical, the effect might be driven by a profile averaged increase of n_e, accompanied by the reduced T_e profile gradients, both effects improving the impurity confinement. Note however, that the additional impact of the strong non neoclassical transport mechanisms observed at W7-X[12,32,40] as well as its determining physics quantities is still under investigation and needs further clarification.

V. SUMMARY

In this work the impurity and energy confinement scaling of purely ECR heated plasmas has been investigated in two different magnetic configurations of W7-X. The scaling of τ_I and τ_E with respect to P_{ECRH} and n_e both follows a simple power scaling law (Eq.1). On average, the energy confinement is slightly enhanced over the impurity confinement ($\tau_E/\tau_I = 1.3$) with observed absolute values of τ_I=40-130 ms and τ_E=40-190 ms. A comparison of the magnetic standard with the high mirror configuration shows a better energy confinement of the standard configuration, as predicted by neoclassical theory while the impurity confinement is very similar for both configurations. Actually, a more detailed analysis of the here obtained results based on neoclassical theory alone is challenging, as recent results show a significant impact of anomalous transport additionally to the neoclassical transport for both the energy[32] as well as the impurity transport[12,40]. Here, detailed investigations on the underlying mechanisms are currently ongoing.

A change in the ECR heating power deposition profile induces a significant change in the impurity confinement, most probably related to the well known enhanced impurity pump out induced by central ECR heating[5,41].

VI. ACKNOWLEDGMENTS

This work has been carried out within the framework of the EUROfusion Consortium and has received funding from the Euratom research and training programme 2014-2018 under grant agreement No 633053. The views and opinions expressed herein do not necessarily reflect those of the European Commission.

[1] J. Garcia-Regana, C. Beidler, R. Kleiber, P. Helander, A. Mollen, J. Alonso, M. Landreman, H. Maaßberg, H. Smith, Y. Turkin, and J. Velasco, Nuclear Fusion **57**, 056004 (2017).

[2] P. Helander, S. L. Newton, A. Mollén, and H. M. Smith, Phys. Rev. Lett. **118**, 155002 (2017).

[3] E. Scavino, J. Bakos, H. Weisen, and T. Team, Plasma Physics and Controlled Fusion **46**, 857 (2004).

[4] Y. Nakamura, Y. Takeiri, R. Kumazawa, M. Osakabe, T. Seki, B. Peterson, K. Ida, H. Funaba, M. Yokoyama, N. Tamura, A. Komori, S. Morita, K. Sato, K. Narihara, S. Inagaki, T. Tokuzawa, S. Masuzaki, J. Miyazawa, N. Noda, T. Mutoh, T. Shimozuma, K. Kawahata, Y. Oka, H. Suzuki, N. Ohyabu, T. Akiyama, N. Ashikawa, M. Emoto, P. Goncharov, M. Goto, H. Idei, K. Ikeda, S. Imagawa, M. Isobe, O. Kaneko, H. Kawazome, K. Khlopenkov, T. Kobuchi, A. Kostrioukov, S. Kubo, Y. Liang, T. Minami, T. Morisaki, S. Murakami, S. Muto, K. Nagaoka, Y. Nagayama, H. Nakanishi, Y. Narushima, K. Nishimura, T. Notake, H. Nozato, S. Ohdachi, S. Okamura, T. Ozaki, A. Sagara, T. Saida, K. Saito, S. Sakakibara, R. Sakamoto, M. Sasao, M. Sato, M. Shoji, N. Takeuchi, K. Tanaka, M. Tanaka, K. Toi, Y. Torii, K. Tsumori, K. Watanabe, T. Watari, Y. Xu, H. Yamada, I. Yamada, S. Yamamoto, T. Yamamoto, S. Yoshimura, Y. Yoshimura, M. Yoshinuma, K. Itoh, T. Mito, K. Ohkubo, I. Ohtake, T. Satow, S. Sudo, T. Uda, K. Yamazaki, K. Matsuoka, O. Motojima, Y. Hamada, and M. Fujiwara, Nuclear Fusion **43**, 219 (2003).

[5] R. Dux, R. Neu, A. G. Peeters, G. Pereverzev, A. Mück, F. Ryter, J. Stober, and A. U. Team, Plasma Physics and Controlled Fusion **45**, 1815 (2003).

[6] M. Mattioli, R. Giannella, R. Myrnas, C. Demichelis, B. Denne-Hinnov, T. D. D. Wit, and G. Magyar, Nuclear Fusion **35**, 1115 (1995).

[7] E. S. Marmar, J. E. Rice, and S. L. Allen, Phys. Rev. Lett. **45**, 2025 (1980).

[8] Y. Nakamura, N. Tamura, M. Yoshinuma, C. Suzuki, S. Yoshimura, M. Kobayashi, M. Yokoyama, M. Nunami, M. Nakata, K. Nagaoka, K. Tanaka, B. Peterson, K. Ida, M. Osakabe, T. Morisaki, and the LHD Experiment Group, Nuclear Fusion **57**, 056003 (2017).

[9] Y. Nakamura, M. Kobayashi, S. Yoshimura, N. Tamura, M. Yoshinuma, K. Tanaka, C. Suzuki, B. J. Peterson, R. Sakamoto, T. Morisaki, and the LHD Experiment Group, Plasma Physics and Controlled Fusion **56**, 075014 (2014).

[10] A. Langenberg, N. A. Pablant, T. Wegner, P. Traverso, O. Marchuk, T. Bräuer, B. Geiger, G. Fuchert, S. Bozhenkov, E. Pasch, O. Grulke, F. Kunkel, C. Killer, D. Nicolai, G. Satheeswaran, K. P. Hollfeld, B. Schweer, T. Krings, P. Drews, G. Offermanns, A. Pavone, J. Svensson, J. A. Alonso, R. Burhenn, and R. C. Wolf, Review of Scientific Instruments **89**, 10G101 (2018).

[11] T. Wegner, B. Geiger, F. Kunkel, R. Burhenn, T. Schröder, C. Biedermann, B. Buttenschön, G. Cseh, P. Drews, O. Grulke, K. Hollfeld, C. Killer, G. Kocsis, T. Krings, A. Langenberg, O. Marchuk, U. Neuner, D. Nicolai, G. Offermanns, N. A. Pablant, K. Rahbarnia, G. Satheeswaran, J. Schilling, B. Schweer, T. Szepesi, and H. Thomsen, Review of Scientific Instruments **89**, 073505 (2018), https://doi.org/10.1063/1.5037543.

[12] A. Langenberg, N. Pablant, O. Marchuk, D. Zhang, J. Alonso, R. Burhenn, J. Svensson, P. Valson, D. Gates, M. Beurskens, R. Wolf, and the W7-X Team, Nuclear Fusion **57**, 086013 (2017).

[13] K. Zhang, Z.-Y. Cui, P. Sun, C.-F. Dong, W. Deng, Y.-B. Dong, S.-D. Song, M. Jiang, Y.-G. Li, P. Lu, and Q.-W. Yang, Chinese Physics B **25**, 065202 (2016).

[14] J. Arevalo, J. A. Alonso, K. J. McCarthy, and J. L. Velasco, Nuclear Fusion **53**, 023003 (2013).

[15] S. Menmuir, L. Carraro, A. Alfier, F. Bonomo, A. Fassina, G. Spizzo, and N. Vianello, Plasma Physics and Controlled Fusion **52**, 095001 (2010).

[16] M. Leigheb, M. Romanelli, L. Gabellieri, L. Carraro, M. Mattioli, C. Mazzotta, M. E. Puiatti, L. Lauro-Taroni, M. Marinucci, S. Nowak, L. Panaccione, V. Pericoli, P. Smeulders, O. Tudisco, C. Sozzi, M. Valisa, and the FTU team, Plasma Physics and Controlled Fusion **49**, 1897 (2007).

[17] O. Marchuk, M. Z. Tokar, G. Bertschinger, A. Urnov, H. . J. Kunze, D. Pilipenko, X. Loozen, D. Kalupin, D. Reiter, A. Pospieszczyk, W. Biel, M. Goto, and F. Goryaev, Plasma Physics and Controlled Fusion **48**, 1633 (2006).

[18] R. Burhenn, J. Baldzuhn, R. Brakel, H. Ehmler, L. Giannone, P. E. Grigull, J. Knauer, M. Krychowiak, M. Hirsch, K. Ida, H. Maassberg, G. K. McCormick, E. Pasch, H. Thomsen, A. Weller, and the W7-AS Team, Fusion Science and Technology **46**, 115 (2004), https://doi.org/10.13182/FST04-A547.

[19] N. A. Pablant, A. Langenberg, A. Alonso, C. D. Beidler, M. Bitter, S. Bozhenkov, R. Burhenn, M. Beurskens, L. Delgado-Aparicio, A. Dinklage, G. Fuchert, D. Gates, J. Geiger, K. W. Hill, U. Höfel, M. Hirsch, J. Knauer, A. Krämer-Flecken, M. Landreman, S. Lazerson, H. Maaßberg, O. Marchuk, S. Massidda, G. H. Neilson, E. Pasch, S. Satake, J. Svennson, P. Traverso, Y. Turkin, P. Valson, J. L. Velasco, G. Weir, T. Windisch, R. C. Wolf, M. Yokoyama, D. Zhang, and the W7-X Team, Physics of Plasmas **25**, 022508 (2018), https://doi.org/10.1063/1.4999842.

[20] T. Klinger, A. Alonso, S. Bozhenkov, R. Burhenn, A. Dinklage, G. Fuchert, J. Geiger, O. Grulke, A. Langenberg, M. Hirsch, G. Kocsis, J. Knauer, A. Krämer-Flecken, H. Laqua, S. Lazerson, M. Landreman, H. Maaßberg, S. Marsen, M. Otte, N. Pablant, E. Pasch, K. Rahbarnia, T. Stange, T. Szepesi, H. Thomsen, P. Traverso, J. L. Velasco, T. Wauters, G. Weir, T. Windisch, and the W7-X Team, Plasma Physics and Controlled Fusion **59**, 014018 (2017).

[21] N. A. Pablant, M. Bitter, R. Burhenn, L. Delgado-Aparicio, R. Ellis, D. Gates, M. Goto, K. W. Hill, A. Langenberg, S. Lazerson, M. Mardenfeld, S. Morita, G. H. Neilson, and T. Oishi, in *41st EPS conference, ECA*, Vol. 38F (2014) p. 1.076.

[22] T. Andreeva, "Vacuum magnetic configurations of Wendelstein 7-X," Tech. Rep. (Max-Planck-Institut für Plasmaphysik, Garching, 2002).

[23] A. Langenberg, J. Svensson, H. Thomsen, O. Marchuk, N. A. Pablant, R. Burhenn, and R. C. Wolf, Fusion Science and Technology **69**, 560 (2016), http://dx.doi.org/10.13182/FST15-181.

[24] J. Svensson and A. Werner, in *International Symposium on Intelligent Signal Processing-WISP* (2007) pp. 955–960.

[25] J. Geiger, C. D. Beidler, Y. Feng, H. Maaßberg, N. B. Marushchenko, and Y. Turkin, Plasma Physics and Controlled Fusion **57**, 014004 (2015).

[26] G. Fuchert, S. Bozhenkov, R. Burhenn, M. Jakubowski, H. Niemann, E. Pasch, T. S. Pedersen, D. Zhang, R. C. Wolf, G. A. Wurden, and the Wendelstein 7-X Team, in *2017 European Conference on Circuit Theory and Design (ECCTD)* (2017) pp. 1–4.

[27] A. Dinklage, C. Beidler, P. Helander, G. Fuchert, H. Maassberg, K. Rahbarnia, T. Sunn Pedersen, Y. Turkin, and R. C. Wolf, Nature Physics **14**, 855 (2018).

[28] B. P. van Milligen, B. A. Carreras, C. Hidalgo, and A. Cappa, Physics of Plasmas **25**, 062503 (2018), https://doi.org/10.1063/1.5029881.

[29] H. Yamada, S. Murakami, K. Yamazaki, O. Kaneko, J. Miyazawa, R. Sakamoto, K. Watanabe, K. Narihara, K. Tanaka, S. Sakakibara, M. Osakabe, B. Peterson, S. Morita, K. Ida, S. Inagaki, S. Masuzaki, T. Morisaki, G. Rewoldt, H. Sugama, N. Nakajima, W. Cooper, T. Akiyama, N. Ashikawa, M. Emoto, H. Funaba, P. Goncharov, M. Goto, H. Idei, K. Ikeda, M. Isobe, K. Kawahata, H. Kawazome, K. Khlopenkov, T. Kobuchi, A. Komori, A. Kostrioukov, S. Kubo, R. Kumazawa, Y. Liang, T. Minami, S. Muto, T. Mutoh, Y. Nagayama, Y. Nakamura, H. Nakanishi, Y. Narushima, K. Nishimura, N. Noda, T. Notake, H. Nozato, S. Ohdachi, N. Ohyabu, Y. Oka, T. Ozaki, A. Sagara, T. Saida, K. Saito, M. Sasao, K. Sato, M. Sato, T. Seki, T. Shimozuma, M. Shoji, H. Suzuki, Y. Takeiri, N. Takeuchi, N. Tamura, K. Toi, T. Tokuzawa, Y. Torii, K. Tsumori, T. Watanabe, T. Watari, Y. Xu, I. Yamada, S. Yamamoto, T. Yamamoto, M. Yokoyama, Y. Yoshimura, M. Yoshinuma, T. Mito, K. Itoh, K. Ohkubo, I. Ohtake, T. Satow, S. Sudo, T. Uda, K. Matsuoka, and O. Motojima, Nuclear Fusion **43**, 749 (2003).

[30] R. Burhenn, Y. Feng, K. Ida, H. Maassberg, K. McCarthy, D. Kalinina, M. Kobayashi, S. Morita, Y. Nakamura, H. Nozato, S. Okamura, S. Sudo, C. Suzuki, N. Tamura, A. Weller, M. Yoshinuma, and B. Zurro, Nuclear Fusion **49**, 065005 (2009).

[31] K. Rahbarnia, H. Thomsen, U. Neuner, J. Schilling, J. Geiger, G. Fuchert, T. Andreeva, M. Endler, D. Hathiramani, T. Bluhm, M. Zilker, B. B. Carvalho, and A. Werner, Nuclear Fusion **58** (2018).

[32] G. Fuchert, S. Bozhenkov, N. Pablant, K. Rahbarnia, Y. Turkin, A. Alonso, T. Andreeva, C. Beidler, M. Beurskens, A. Dinklage, J. Geiger, M. Hirsch, U. Höfel, J. Knauer, A. Langenberg, H. Laqua, H. Niemann, E. Pasch, T. S. Pedersen, T. Stange, J. Svensson, H. T. Mora, G. Wurden, D. Zhang, R. Wolf, and the W7-X Team, Nuclear Fusion **58**, 106029 (2018).

[33] S. Marsen, Y. Corre, H. Laqua, V. Moncada, D. Moseev, H. Niemann, M. Preynas, T. Stange, and the W7-X Team, Nuclear Fusion **57**, 086014 (2017).

[34] U. Stroth, T. Geist, J. P. T. Koponen, H.-J. Hartfuß, P. Zeiler, ECRH, and the W7-AS Team, Phys. Rev. Lett. **82**, 928 (1999).

[35] R. Wolf, S. Bozhenkov, A. Dinklage, G. Fuchert, H. Laqua, S. Marsen, N. B. Marushchenko, T. Stange, M. Zanini, I. Abramovic, A. Alonso, J. Baldzuhn, M. Beurskens, C. D. Beidler, H. Braune, K. J. Brunner, N. Chaudhary, H. Damm, G. Gantenbein, J. Geiger, M. Hirsch, U. Hoefel, J. Jelonnek, Y. O. Kasakov, W. Kasparek, J. Knauer, A. Langenberg, C. Lechte, H. Trimino Mora, U. Neuner, D. Moseev, O. H., N. Pablant, E. Pasch, B. Plaum, T. Sunn Pedersen, K. Rhabarnia, J. Schilling, E. Scott, H. Thomsen, M. Thumm, Y. Turkin, and F. Wilde, "Electron-cyclotron-resonance heating in Wendelstein 7-X: A versatile heating and current-drive method and a tool for in-depth physics studies," (2018), submitted for publication.

[36] S. Bozhenkov, M. Beurskens, A. D. Molin, G. Fuchert, E. Pasch, M. Stoneking, M. Hirsch, U. Höfel, J. Knauer, J. Svensson, H. T. Mora, and R. Wolf, Journal of Instrumentation **12**, P10004 (2017).

[37] E. Pasch, M. N. A. Beurskens, S. A. Bozhenkov, G. Fuchert, J. Knauer, and R. C. Wolf, Re-

view of Scientific Instruments **87**, 11E729 (2016), http://aip.scitation.org/doi/pdf/10.1063/1.4962248.
[38]P. Helander, C. D. Beidler, T. M. Bird, M. Drevlak, Y. Feng, R. Hatzky, F. Jenko, R. Kleiber, J. H. E. Proll, Y. Turkin, and P. Xanthopoulos, Plasma Physics and Controlled Fusion **54**, 124009 (2012).
[39]M. Grahl and J. Geiger, "Web service access on data of vmec equilibrium calculations for W7-X," https://svvmec1.ipp-hgw.mpg.de:8080/vmecrest/v1/geiger/ (2018).
[40]B. Geiger, T. Wegner, R. Burhenn, B. Buttenschön, A. Langenberg, T. Puetterich, R. Dux, T. Windisch, G. Fuchert, N. Pablant, Y. Turkin, C. Beidler, P. Traverso, and V. Winters, "Observation of anomalous impurity transport in Wendelstein 7-X," (2018), submitted for publication.
[41]N. Tamura, C. Suzuki, S. Satake, Y. Nakamura, M. Nunami, H. Funaba, K. Tanaka, M. Yoshinuma, K. Ida, and S. Sudo, Physics of Plasmas **24**, 056118 (2017), https://doi.org/10.1063/1.4983626.